ANDOR
an Oxford Instruments company

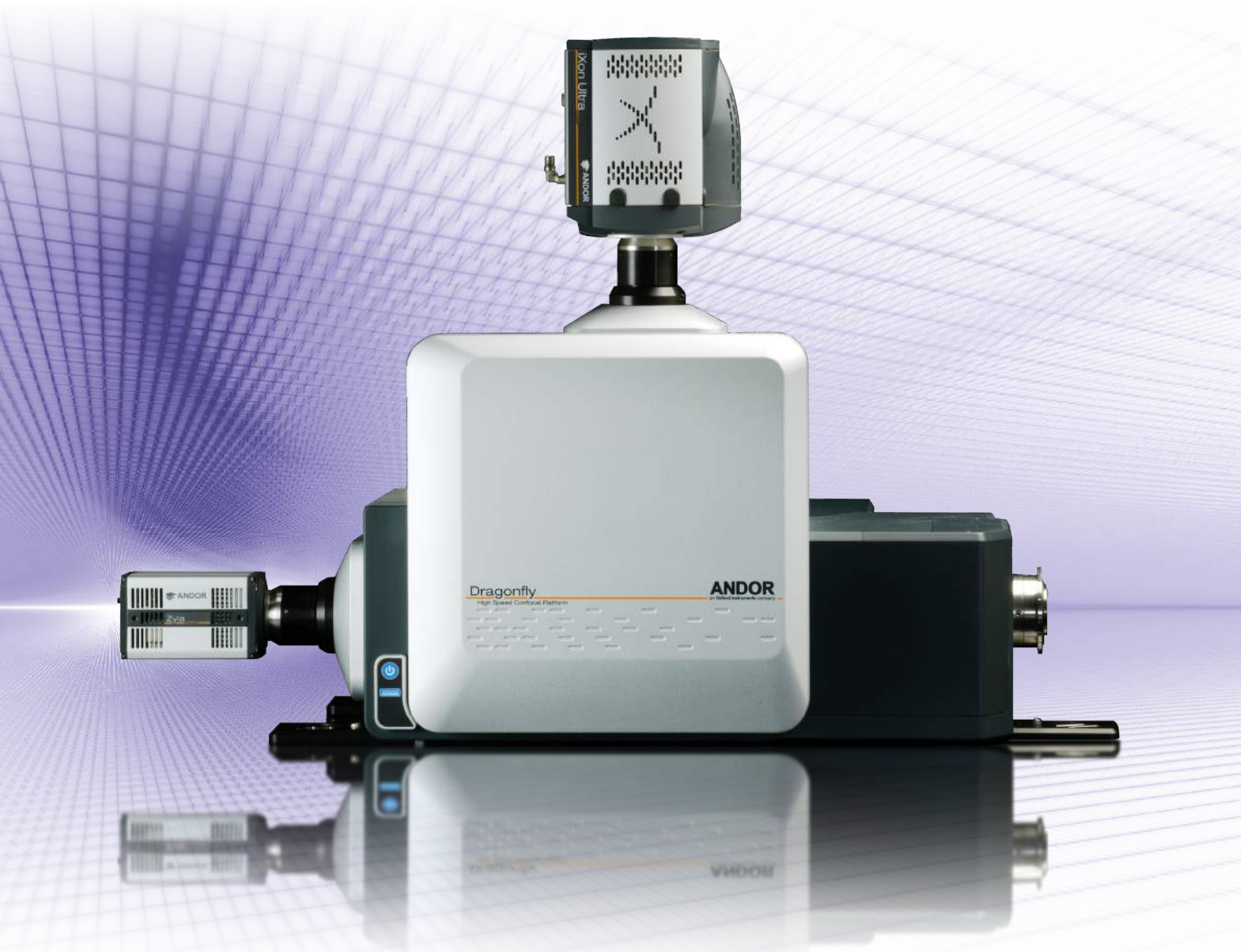

Twelve Reasons Why

Your Next Confocal Should Be Dragonfly

Dragonfly
It's more than confocal...

Twelve Reasons Why Your Next Confocal Should Be Dragonfly

Andor's Dragonfly High Speed Confocal Platform offers outstanding performance and flexibility, so when your research calls for confocal, consider these twelve compelling reasons why Dragonfly should be next in your lab or core facility. Bottom-line, Dragonfly delivers: **productivity, speed, sensitivity, extended spectral range and quantifiable results.**

Dragonfly, Andor's High Speed Confocal is driven by Fusion software, showing volume rendering of 2048 x 2048 x 821 voxels of a fixed zebra fish embryo; the full thickness of 157 µm was acquired in 3 channels and a 0.19 µm Z step. Fusion features a modern intuitive user interface, real-time volume visualization, high performance multi-dimensional acquisition, GPU-accelerated deconvolution and an increasing array of tools to: Acquire, Visualize, Analyze. Fusion acquires in native IMS (Imaris) files format and supports multi-terabyte data sets with seamless delivery to the advanced image and data analysis tools of Imaris.

IN A HURRY? – SPEED READ. If you don't have time to read the full article scan this table for twelve compelling reasons to consider Dragonfly, the brand new high speed confocal platform from Andor.

1	At least 10 times faster than point scanning confocals, even resonant scanners: get more done!
2	3–5 times more sensitive than typical point scanning confocals, benefiting from the latest sCMOS and EMCCD detectors: visualize low fluorophore density and speed imaging times.
3	Background rejection – Dragonfly sets new performance standards for background rejection, routinely imaging specimens spanning hundreds of microns axially.
4	Resolution – Dragonfly matches point scanners for lateral and axial resolution: with motorized zoom and pinhole selection, several objectives can be used at or above diffraction limited imaging.
5	99% linearity, simplifies quantitative imaging: in contrast point scanners tend to saturate fluorophores leading to non-linearities.
6	Dynamic range – 10–100 times that of point scanning confocals, allowing visualization and quantification of bright and dim features in a single scan.
7	Gentler imaging – Dragonfly scans thousands of microbeams for reduced photobleaching and phototoxicity, enabling better imaging of delicate specimens.
8	Greater spectral range – VIS-NIR (400–800 nm), supporting greater multiplexing and lower tissue absorption and scattering for thicker specimens.
9	Excellent image uniformity – Andor's patented Borealis™ illumination supports a large field of view (22 mm diagonal) and provides benefits for quantitative imaging and/or image stitching.
10	Enhanced excitation stability – Andor's patented Borealis™ illumination uses a large diameter multi-mode fiber to reduce the impact of thermal and mechanical drift; a larger fiber lowers risk of damage and contamination, simplifying alignment and reducing maintenance.
11	dSTORM– Dragonfly supports direct-STORM. Motorized Borealis™ illumination zoom achieves high power density for single molecule localization microscopy.
12	SRRF (super-resolution radial fluctuations) – Dragonfly supports this new algorithm with resolution similar or better than structured illumination microscopy (SIM) for use with conventional fluorophores. SRRF functions with confocal, TIRF and wide field imaging modes.

Abstract

Dragonfly is a high performance multi-modal imaging platform. In this article, we focus on Dragonfly's multi-point scanning confocal imaging performance and compare it to single point scanning, which has become the dominant technology over the last 30 years. We show that Dragonfly exceeds or matches the performance of point scanners in all important aspects. As life science research accelerates and demands greater throughput for deeper study, we suggest the community should consider this new and powerful platform wherever there is a need for fast, sensitive, high resolution confocal imaging.

REASON ONE: Speed

Dragonfly is ten to twenty times faster.

Point scanning confocal microscopes, like those provided by the major microscope companies, have become the de facto standard for fixed cell and tissue imaging and they can be stretched to some live cell work. But sequential scanning of a single beam through millions or billions of voxels (volume elements) is a laborious process with major disadvantages (Pawley 2000). In contrast the multi-point scanning methodology used in Dragonfly, scans thousands of micro-beams to deliver parallel confocal imaging. In head to head comparisons with the latest point scanners, Dragonfly delivers 10–20 times faster volumetric imaging and, as we shall show, this is achieved with the highest quality.

Perhaps surprisingly, the speed comparison holds true even for resonant scanning systems, because the speed limitation cannot be overcome simply by scanning a single beam faster. The ultimate limitation boils down to the number of photons that can be collected from a diffraction limited volume in a single voxel dwell time (Tsien et al 2006): faster single beam scanning requires either increasing beam power, or frame averaging for adequate signal to noise ratio. The former rapidly bleaches fluorophores with damaging side-effects (phototoxicity), while the latter slows the acquisition rate. Typical acquisition rates for resonant scanners are 512x512 voxels at 30 frames per second (fps).

Dragonfly's multi-point scanning is based on microlens spinning disk (MSD) technology. MSD was exclusively used in the Yokogawa confocal scanning unit (CSU) until the introduction of Andor's new instrument. Key features of MSD technology include high scan rates (200–2000 scans per second), no dead time while scanning, unlike point scanners, and support for extremely sensitive detectors. Because MSD scans the specimen continuously when illuminated, it is easy to adjust frame rate by controlling camera exposure time and synchronizing laser illumination: during an exposure, signal is integrated over one or more scans onto a high sensitivity, fast readout camera. Dragonfly's underlying scan rate is 400 scans per second, making it possible to image with incremental exposures of 2.5 ms. Paired with an sCMOS camera, Dragonfly can deliver up to 400 fps at 512x512 resolution.

While point-scanners can be configured for parallel detection of multi-channel fluorescence to improve speed, results may be negatively impacted by spectral cross-talk between fluorophore channels and increased photobleaching. To correct for this cross-talk, "spectral detection" (Dickinson et al 2001) can be used to separate overlapping fluorophore emissions.

However, this results in reduced signal to noise ratio (SNR) because the signal must be split over an array of detectors and each detector element has an associated read noise. To a good approximation, signal per channel will be reduced by the number of channels, C, in a spectral band and the read noise (RN) will increase as $C^{1/2}$, so that signal to noise ratio (SNR) for a fixed number of photons N will be, $SNR = N/(C*(N+RN^2))^{1/2}$. The imaging rate must usually be slowed to achieve adequate SNR for the linear unmixing algorithms to do their job, but with sufficient SNR, these tools can perform extremely well.

The smartest approach to minimizing spectral cross-talk in a multi-channel MSD instrument is to use pair-wise simultaneous acquisition where the excitation and emission wavelengths are well separated. For example, a four-wavelength experiment might proceed with laser excitation of pairs 405 & 560 followed by 488 & 640 nm to achieve low cross-excitation and higher speed. In this scenario, SNR is not impacted and cross talk is minimized. Dragonfly supports this kind of simultaneous dual-channel imaging with two cameras, providing a potential frame rate of 800 frames (400 image pairs) per second.

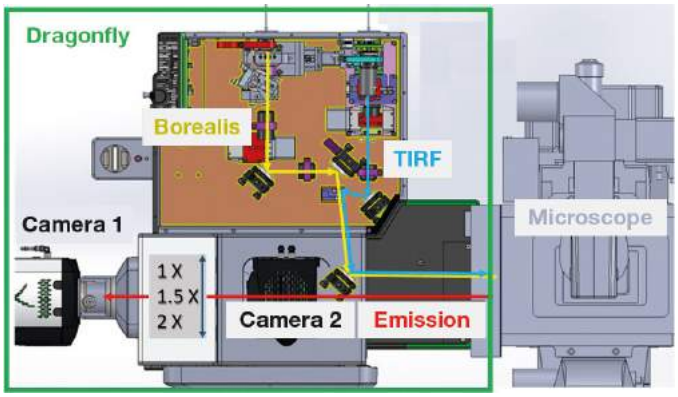

Figure 1. Schematic showing light paths in Dragonfly. Borealis™ zoom illumination provides enhanced throughput, uniformity and spectral range for confocal and epi-fluorescence imaging. TIRF (total internal reflection fluorescence) illumination enables simultaneous multi-wavelength control of penetration depth. Each Dragonfly is optimized for its companion microscope. On the detection side, dual cameras can be used with three zoom settings on each. To enable simultaneous image capture, a motorized quad image splitter and dual 8-position filter wheels support high performance imaging across a wide range of applications. For flexibility and ease of use the filter wheels have embedded RFID (radio frequency identification) which allows Dragonfly to adapt automatically to different filter configurations.

REASON TWO: Sensitivity

Dragonfly is 3–5 times more sensitive

Sensitivity is critical to all microscopic imaging studies because it is a measure of the light budget (efficiency) between specimen and instrument and determines the minimum detectable signal. Critical factors affecting sensitivity are quantum efficiency (QE) and read noise (RN) of the detector as well as instrumental and measurement background (specified here by mean and variance, var). In 2-D detectors, as the limits of performance are reached, fixed pattern noise (FPN) becomes an important parameter. Tiny variations in sensitivity across the sensor material, give rise to a low level structured background, sometimes referred to as photo-response non-uniformity (PRNU). Camera manufacturers go to great lengths to correct PRNU and minimize its impact.

The theoretical limit to SNR is shot noise resulting from the statistical nature of photon emission. The absolute maximum SNR is $N^{1/2}$ or square root of the number of detected photons, so the more photons that can be gathered, the better the SNR. QE measures the efficiency of a detector to convert photons incident upon it, to photo-electrons (signal). Instrumental SNR for a given number of incident photons, N can therefore be summarized as follows:

$$SNR = \frac{(N*QE\text{-mean(background)})}{(N*QE+FPN^2+RN^2+\text{var (background)})^{1/2}} \quad \text{Equation 1}$$

Point scanners utilize photomultiplier tubes (PMTs) for detection and consequently are limited by the QE of the photocathode materials used in these devices. Typical QE values of PMTs in high end instruments are 10–40% depending on wavelength and photocathode material (Hamamatsu 2007). Gallium Arsenide Phosphide (GaAsP) photocathodes provide the highest QE, exceeding 25% from 400–650 nm with rapid decline outside this region and a peak of 40% at 540 nm (see Figure 2). The PMT relies on electron multiplication through a dynode chain and this introduces multiplicative noise (MN). Assuming good design, MN increases noise by a factor of around 1.25, which is equivalent to reducing QE by a factor of MN^2 or about 1.56. Hence the effective peak QE of a GaAsP detector is approximately 26%. Moreover, the system SNR is inversely proportional to the square root of the detection circuit bandwidth, which provides another challenge for speeding acquisition with resonant scanning, where bandwidth increases by a factor of 10 or more.

A more recent development is the use of hybrid detectors (HyD) (Hamamatsu 2007), which combine GaAsP photocathode with direct acceleration of the resulting electrons into a silicon avalanche diode (AD). The resulting gain is much lower than a PMT and is highly dependent on temperature, but the MN problems of a dynode chain are reduced and the HyD has benefits in terms of pulse height repeatability and stability. Although these detectors are often quoted for use in photon counting mode (PCM), it is worth pointing out that PCM of 512x512 voxels at 30 fps with 12-bit resolution would require a PCM bandwidth of ~$4x10^{10}$ pulses per second. These bandwidths are achieved in specialized TCSPC (time-correlated single photon counting systems) (Becker 2005), but as far as we know are not common in commercial point scanners. Insufficient PCM bandwidth results in pulse pile-up and non-linearity, especially in high signal conditions and this impacts linearity (see Reason Four).

In contrast, Dragonfly utilizes the latest generation back side illuminated (BSI) electron multiplying charge coupled devices (EMCCD) and Scientific Complementary Metal Oxide Semiconductor (sCMOS) sensors with peak QEs between 82% and 95% and broad spectral profiles (300–950 nm). The effective read noise of an EMCCD is estimated from output amplifier read noise divided by the EM Gain. Thus, Andor's iXon Ultra 888 can deliver read noise of < 0.2 electrons rms (root mean square) (Basden 2015). EMCCD's show multiplicative noise (MN) in the gain register, like PMT's, but thanks to the very low effective read noise, deliver single photon sensitivity. EMCCD MN is typically 1.41, resulting in an effective peak QE of about 48%, but this is still almost twice that of the best PMT with a substantially wider spectral range (see Figure 2).

SCMOS detectors were first introduced by Andor in 2009 (Coates et al 2009). The major benefit of sCMOS is the ability to implement sophisticated circuitry on the same chip as the photo sensor array. This allows parallel readout and digitization of all rows and/or columns of the sensor. For example, a 2048x2048 sensor (4 Mpixel) can be read at 100 fps, while each pixel is addressed at only 200 kHz and thus a very low readout noise, e.g. 1–2 electrons rms, can be achieved. Since read noise is critical to sensitivity, this performance at high QE gives Dragonfly a significant advantage over point scanning instruments.

However, EMCCD remains the most sensitive detector at low signal levels (20–30 photons per pixel). In Figure 3, we compare EMCCD and sCMOS operating in Dragonfly under near identical imaging conditions, while increasing the exposure time and hence photon count, to illustrate relative imaging performance.

Comparing EMCCD and sCMOS detectors to PMT's by effective QE, results in an advantage to Dragonfly of three to five times.

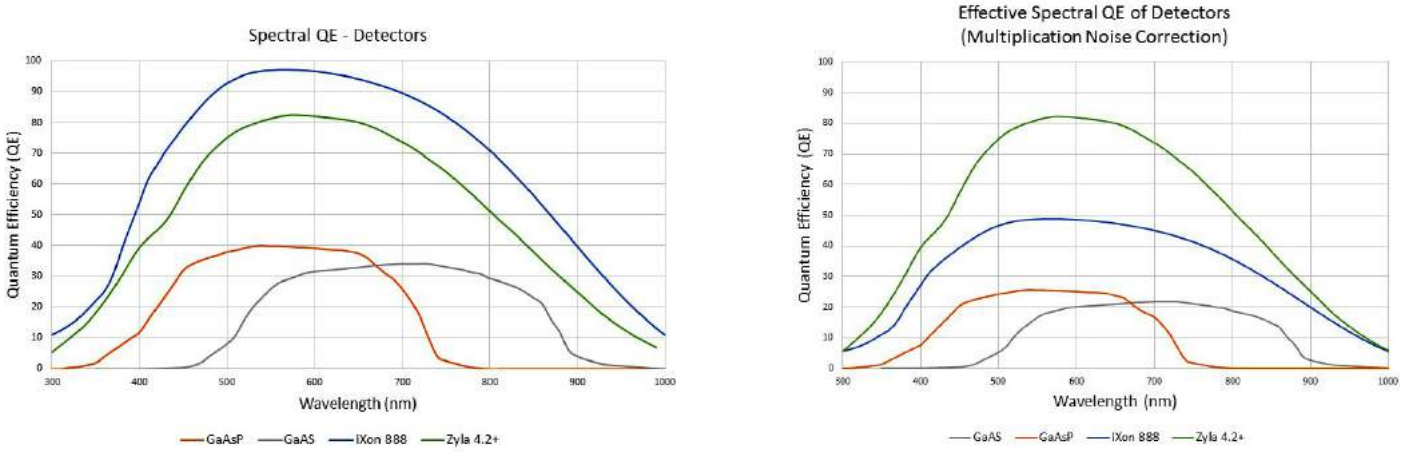

Figure 2. Detector performance sets the baseline for instrument sensitivity. Above left we show the QE of PMT's vs EMCCD and sCMOS detectors. On the right, we account for multiplicative noise, which is modeled as a reduction in QE by the square of the noise factor.

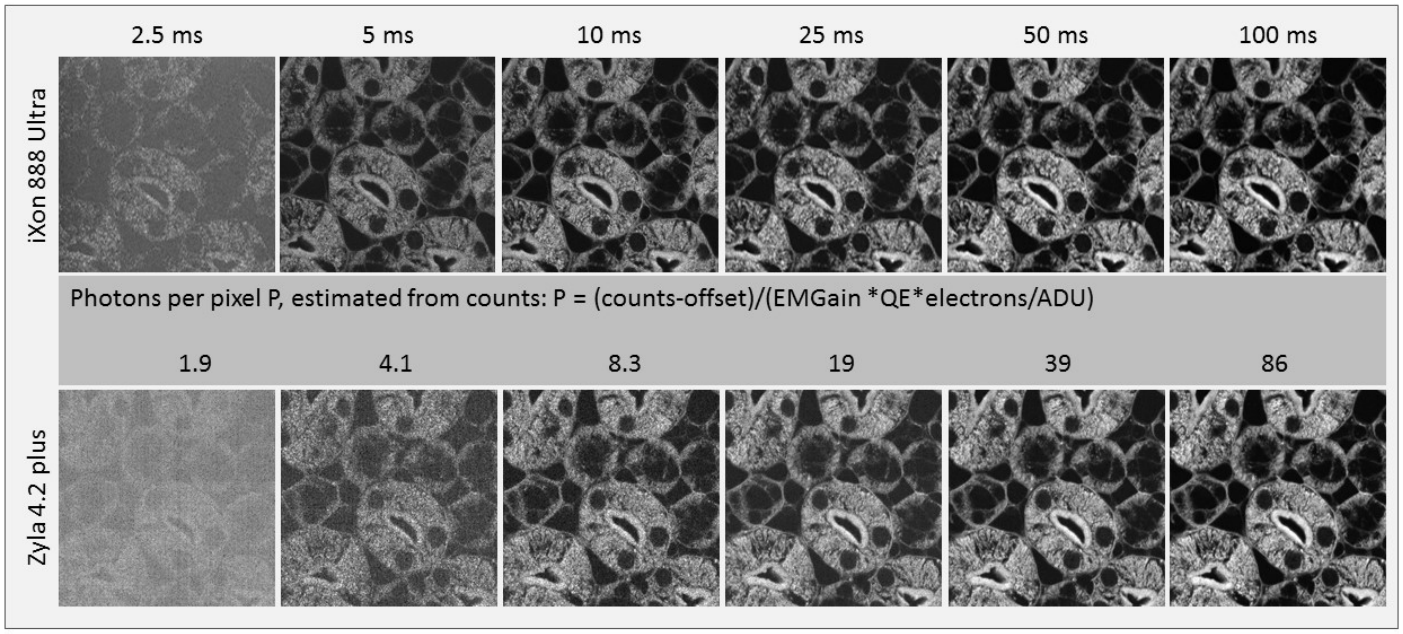

Figure 3. iXon Ultra EMCCD and Zyla 4.2 plus sCMOS cameras were directly compared for sensitivity: cameras were set up on the imaging ports of Dragonfly and were pixel size matched using imaging zoom: Zyla at 1X and iXon at 2X resulting in a pixel size of 6.5 µm. The same specimen was sequentially imaged onto each camera with exposures interleaved (Zyla:iXon:Zyla:iXon etc.) so that one camera was not substantially disadvantaged by bleaching. The "cross-over" where sCMOS delivers similar image SNR to EMCCD is between 20 and 30 photons per pixel.

REASON THREE: Imaging thick or high background specimens

In practice Dragonfly rivals point scanners

Although QE is a critical to sensitivity, SNR and contrast can also be limited by non-specific background from the specimen as identified in Equation 1. An instrument's capability to reject such background is then a key parameter. The most demanding scenario, has a "sea of fluorescence" emitting in the out-of-focus volume of the specimen, excited by divergent beams from adjacent pinholes (Egner et al 2000). This is representative of auto-fluorescence in tissue specimens (see Figure 12), but may not be typical of many other specimens which are specifically labelled. Nonetheless, this scenario helps to compare performance between single point scanning and other technologies. In point scanners, there is only a single pinhole so there can be no cross-talk. In MSD and other multi-point scanners, cross-talk between pinholes sets the limit to contrast.

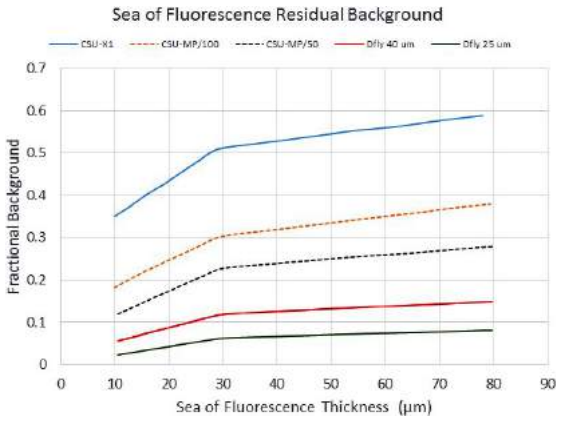

Figure 4. Extended from Shimozawa to include like scaled data for Dragonfly with 40 and 25 µm pinholes. Data was scaled using CSU-X1 as a reference point. Note: CSU-MP (multi-photon) is not available commercially: CSU results shown are from Shimozawa (2013) using single photon excitation.

More specifically, pinhole size, spacing and objective magnification set the depth at which fluorescence from adjacent excitation volumes infiltrates neighboring pinholes. Pinhole size and spacing (open area fraction) also determines the transmission of the pinhole disk, which sets contrast in the sea of fluorescence test. In older MSD, the transmission varies from 4% to 1% and at 60X the pinhole separation in specimen space is between 4 and 8 µm, so that cross-talk begins in specimens above 5 or 10 µm. Shimozawa et al (2013) used the sea of fluorescence test to evaluate the performance of different models of CSU, including multi-photon models. They plotted residual background fraction vs thickness of the sea of fluorescence and in Figure 4 we show their results for single photon performance of CSU models and extend the series for Dragonfly 40 and 25 µm pinholes. Clearly, Dragonfly is between two and ten times more capable at rejecting background in single photon MSD, but as you would expect does not match multi-photon MSD – not shown, but close to zero.

Point scanners show excellent performance in the sea of fluorescence test, but practical comparison with Dragonfly using real specimens yields somewhat surprising results. Slow scanning speed and high bleaching rates, combined with inferior sensitivity result in surprisingly poor imaging performance with thicker specimens. Most researchers have resorted to multi-photon point scanning, but Dragonfly provides an alternative and much faster solution which is attracting interest. In practice, with specifically labelled thick specimens Dragonfly imaging performance has proven exceptional, routinely delivering high contrast in embryos and tissues hundreds of microns thick, as illustrated in Figure 5.

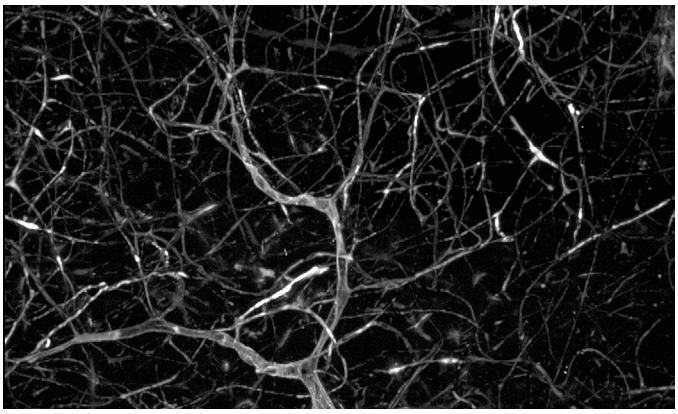

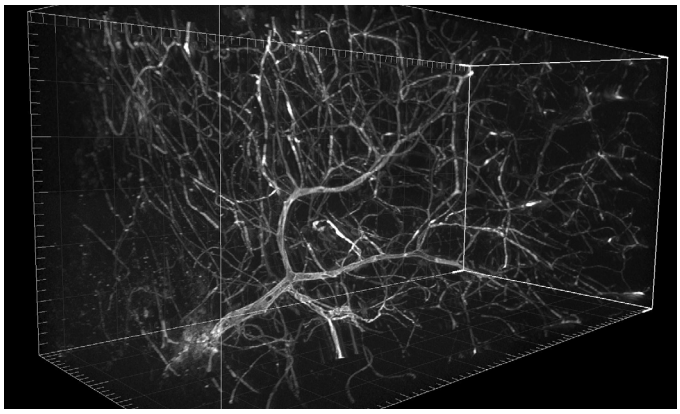

Figures 5a and 5b. Dragonfly image of bead-labelled blood vessels in a mouse brain, cleared by the CUBIC method. A shows a maximum intensity projection of the data, while B show a voxel rendered visualization. Specimen imaged with 40 um pinhole at 561 nm and 620/60 emission filter with 20 X 0.45 dry objective. Field dimensions 620x620x1220 um - 1024x1024x1820 voxels. Specimen courtesy of Dr Alan Watson, University of Pittsburgh. Apparent beyond about 800 µm, spherical aberration and tissue scattering degrade signal and point spread function fidelity, so that greater care must be taken with tissue mounting and lens selection.

REASON FOUR: Resolution

Motorized camera zoom and pinholes support multiple objectives

Received wisdom is that point scanners outperform MSD in terms of lateral and axial resolution. While this may be true of older generation MSD where pinhole size and detector optics were fixed, Dragonfly overcomes this limitation by delivering Nyquist sampling over a range of microscope objectives and provides a choice of pinholes, enabling trade-off between resolution and sensitivity. Further, diffraction limited resolution can be exceeded via a combination of "sub-Airy" pinhole and deconvolution. Fusion deconvolution makes use of a graphics processing unit (GPU) which executes the necessary mathematical functions in a highly parallel manner, achieving 10–20 times faster processing than central processing unit (CPU) based approaches.

With the Dragonfly 500 series, three imaging port magnifications are provided: 1X, 1.5X and 2X. These allow the detector sampling to be adapted to different objectives. Table 1 shows the "strict" Nyquist lateral and axial sampling interval (dXStrict and dZStrict) for confocal imaging, to ensure that all spatial frequencies are sampled (Heintzmann and Sheppard 2007). This formulation is for a noise free system. In practice, noise will most strongly impact the highest frequencies, so we may choose to relax sampling and improve SNR, since the number of photons gathered per pixel increases with the square of the pixel dimension. High SNR is desirable when using deconvolution, but we must not relax sampling too much or we will lose the high frequency information which we try to recover in the process.

Confocal resolution depends not only on detector sampling, but also the illumination/detection pinhole size, as summarized graphically in Figure 6. Equation 2 describe the lateral full width half maximum (LFWHM) response to a point object in the confocal microscope with a point detector. Equation 3 describes the axial (AFWHM) response to a planar fluorescent sheet as it is scanned through focus. Equation 4 shows a good approximation of the relationship between AFWHM and pinhole size in Airy Units (AU) (Wilson 2011).

$$LFWHM = 0.3\ \frac{\lambda}{NA} \quad \text{Equation 2}$$

$$AFWHM = 0.67\ \frac{\lambda}{n-\sqrt{(n^2-NA^2)}} \quad \text{Equation 3}$$

$$AFWHM\ (AU) = 0.67\ \frac{\lambda}{n-\sqrt{(n^2-NA^2)}}\ \sqrt[3]{(1+1.47AU^3)} \quad \text{Equation 4}$$

To scale lateral and axial resolution onto the same axis in Figure 6, take the reciprocal of AFWHM(AU) and LFWHM(AU) and multiply by LFWHM from equation 2. The x axis of Figure 6 is calibrated in Airy units: 1 AU = 1.22λ/NA, and corresponds to the diameter of the first zero in the Airy disk produced when a lens of numerical aperture NA images a point object.

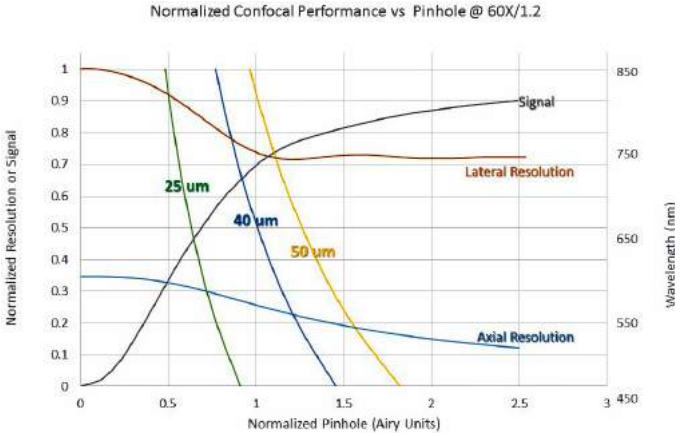

Figure 6. Graphic summarizing normalized Signal, Lateral and Axial Resolution in the confocal microscope. As the pinhole size is reduced, axial and lateral resolution improve. The profiles labelled 50, 40 and 25 um show the loci of pinholes of that dimension and their equivalent Airy-scaled size as wavelength varies – for a 60X/1.2 Water objective. The normalized pinhole radius is inversely proportional to imaging wavelength, scaled on the right-hand Y axis. The Dragonfly 40 um pinhole is near optimum (1 AU) at this magnification, while the 25 µm pinhole achieves enhanced axial and lateral resolution at the cost of signal.

Obj	NA	dXStrict	dZStrict	Image Pixel Size	Mag Zyla	Mag iXon	R Mag Zyla	R Mag iXon
100	1.4	0.04	0.13	4.36	1.49	2.98	1.07	2.14
60	1.2	0.05	0.16	3.05	2.13	4.26	1.52	3.04
60	1.4	0.05	0.14	2.81	2.31	4.62	1.65	3.30
40	1	0.06	0.27	2.44	2.66	5.33	1.90	3.81
25	0.75	0.08	0.53	2.03	3.20	6.39	2.28	4.57

Table 1. Shows "Nyquist" pixel size for different objectives. dXStrict and dZStrict show the strictly computed sampling interval at the specimen plane in a noise free system. Mag Zyla and Mag iXon show the magnification in the camera tube required to achieve strict Nyquist sampling on the relevant camera. Green indicates those cases that meet Nyquist on Dragonfly. R Mag Zyla and R Mag iXon indicate the "relaxed Nyquist" sampling criteria that may be applied to trade signal and resolution.

We see for pinholes below 0.5 AU, that normalized lateral and axial resolutions are close to their maxima, with lateral resolution about 1.3–1.4 times the wide field resolution, described by various criteria including Abbe and Rayleigh limits. With a pinhole of 1.2 AU or larger, the lateral resolution plateaus at the Abbe limit (λ/2NA) with a normalized value of ~0.72, while the axial resolution continues to roll-off with larger pinholes.

The widely accepted "best compromise" for pinhole size, trading resolution and signal, is about 1.0 AU. Larger pinholes offer little benefit because ~70% of the signal (energy) is already captured in the Airy disk and increasing pinhole size mainly passes more out-of-focus light, degrading contrast. Smaller pinholes can improve lateral and axial resolution to a point, and when used with deconvolution can exceed the Abbe limit by a factor of 1.3 to 1.4 – see Figure 7.

A key design goal for Dragonfly was to match the resolution of point scanners and provide flexibility for different objectives. Camera zoom enables Nyquist sampling to be maintained for a range of objectives as illustrated in Table 1. The optimum pinhole for a 60X/1.2 W lens is around 40µm, while optimum for a 40X/1.0 W lens is about 25 µm. At longer wavelengths, Dragonfly's NIR imaging capabilities benefit from the 25 µm pinhole for lower magnifications such as 25X Water or Multi-immersion objectives which are often recommended for imaging thick and cleared tissue.

Beyond the purely optical performance, GPU-accelerated deconvolution provides both lateral and axial resolution enhancement. The reduction in out of focus haze enhances contrast and enables measurements that were previously difficult or impossible. Fusion's deconvolution is fast and can be interleaved with acquisition to ease its use and optimize workflow. Resolution test results are shown Table 2 and Figure 7.

PSF measurements += with Deconvolution	WF Raw	WF+	DFly40	DFly40+	WF Theory
Lateral FWHM(nm)	245	185	238	139	218
Axial FWHM(nm)	573	386	523	248	510
Lateral (XY) projection		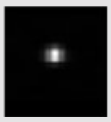		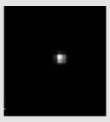	
Axial (Z) projection	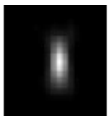	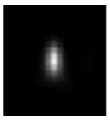	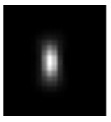	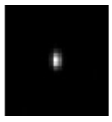	

Table 2. The matrix for comparison of imaging performance with the Dragonfly in widefield and confocal with 40 µm pinhole before and after deconvolution. 25 µm data will be added to this table in the next revision of the white paper. Measurements were made with MetroloJ imageJ plugin for PSF analysis. 100 nm beads fluorescent were imaged at 488 nm laser excitation, with a Zyla 4.2 plus, 1X camera zoom and Nikon 60X/1.4 planapo oil lens, Z step was 0.1 µm.

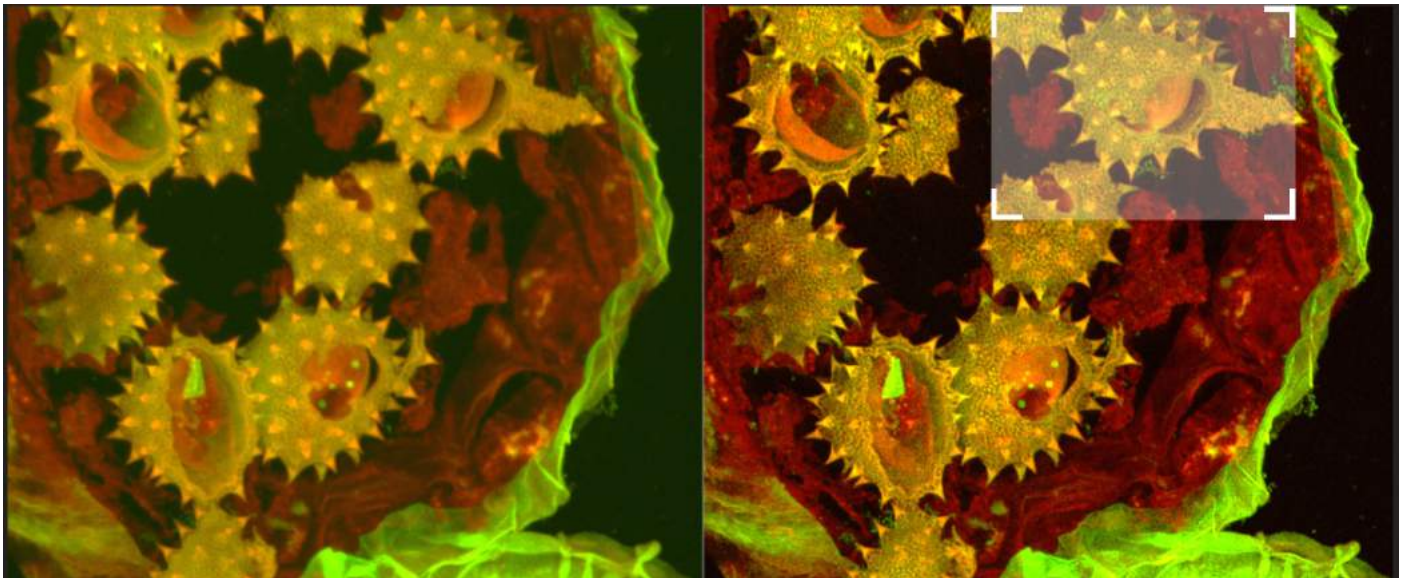

7 A. shows full field image of the daisy pollen grains before and after deconvolution, with merged channels viewed as a maximum intensity projection image. Note the contrast and detail enhancement in the deconvolved images. Because this is a bright robust specimen, we could extend exposure times to 250 ms, achieving high SNR to recover high spatial frequencies for deconvolution. Thus, we could exceed the Abbe diffraction limit in confocal imaging. But the density of the specimen is also a challenge to optical sectioning, as evidenced in the haziness of the single optical section in C. Daisy pollen maximum intensity projection of 488 and 561 channels before and after deconvolution with Fusion.
Blue region shown in detail in 7B below.

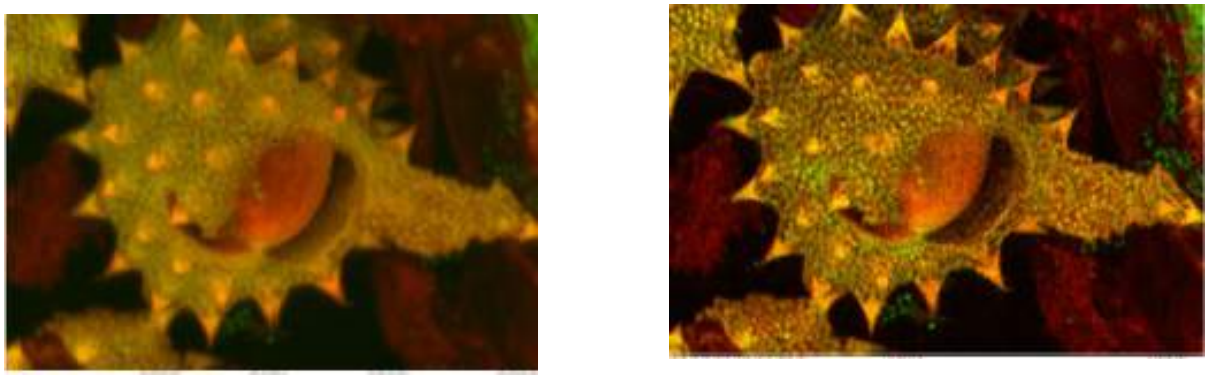

7 B. shows detail at full resolution from image in A above. Surface clarity is enhanced as well as sharpness and resolution improvement in individual pollen grain.

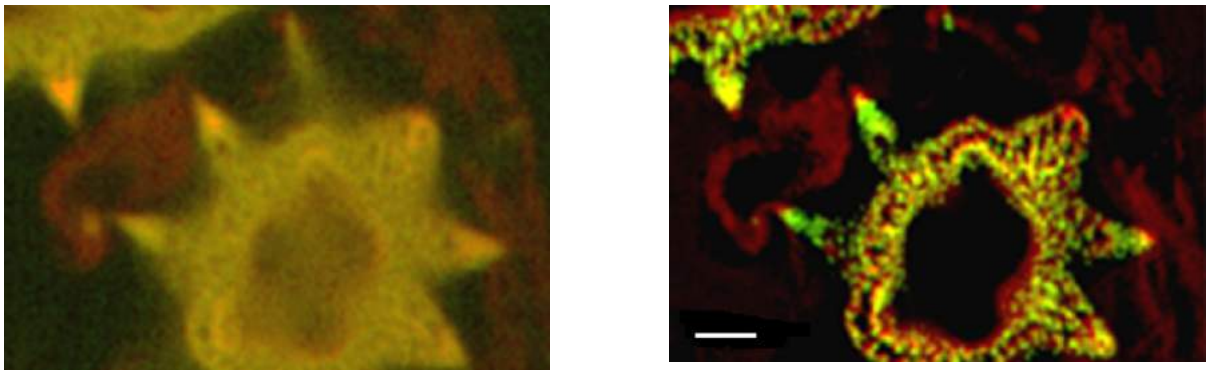

7 C. Single optical section from two channel daisy pollen Z series. Deconvolution enhances contrast, sharpens optical sectioning and provides clear channel separation in this thick bright specimen. Fine structures within the walls of the pollen grains become clearly visible. These punctate features are in the range 150-200 nm FWHM after deconvolution. Scale bar is 2 µm.

Figure 7. Images from a reference specimen: daisy pollen grains were imaged on Dragonfly with 488 and 561 laser excitation. A Zyla 4.2 PLUS was used with 1X camera zoom and Leica 100X/1.44 oil lens.

REASON FIVE: Linearity in Dragonfly is 99% – Point scanners do not quote this parameter

Linearity is important for quantitative studies where, for example, abundance of a fluorophore is used as a proxy for protein quantification or for monitoring dynamics processes like metabolic state or signaling.

Point scanners typically operate close to fluorophore excitation saturation (Tsien et al 2006) and consequently exhibit a non-linear relationship between input power and photon emissions. In addition, as discussed above, PMTs are known to have significant non-linearities at high operating currents (Hamamatsu 2007) so that bright features appear dimmer. These two factors combine to create the typical power/signal curve obtained from a point scanning confocal (after Wang et al 2005) shown in Figure 8. Operating at these power levels also shows high bleaching rates and phototoxicity: we will explore this further below.

In contrast, MSD micro-beam excitation powers are two or three orders of magnitude lower than the single beam instrument. This ensures that each micro-beam is well below saturation and fluorescence linearity is maintained in each of the probed volumes. Dragonfly EMCCD and sCMOS detectors exhibit >99% linearity over a wide dynamic range, operating in 16-bit readout modes and this combined with excitation in the linear range of fluorophores sets the instrument linearity.

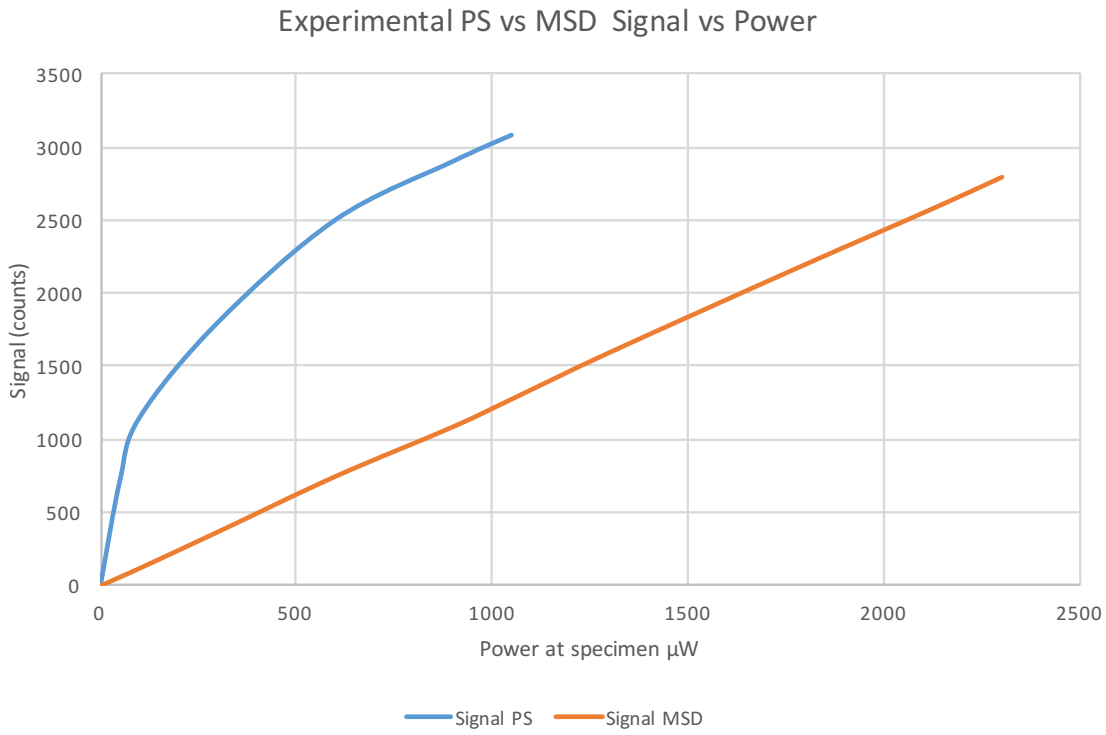

Figure 8. Signal to Power relationship of point scanner (PS) versus microlens spinning disk (MSD) confocal (after Wang et al 2005) with Andor iXon 897 EMCCD camera. Dragonfly uses a unique microlens dual spinning disk design, operating on the same principle as the unit compared by Wang, but with enhanced performance in terms of throughput, field of view and resolution.

REASON SIX: Dynamic Range

Dragonfly up to 15-bit dynamic range versus point scanners 8–12 bits

Saturation and non-linearity in point scanners, combine to produce low dynamic range data, which cannot capture the true range of intensities in a specimen. As an illustration of this point, the reader will note that point scanners often require two scans: one to capture dim signals and one to capture bright signals. Such demands add further to imaging time and bleaching effects. The images can be combined, but due to the low (sensitivity) QE of PMT detectors will never reproduce the dimmest features in the specimen with good signal to noise ratio.

In contrast, Dragonfly's micro-beam scanning combined with high quantum efficiency (QE), linear detectors such as EMCCD or sCMOS, provides linear excitation and detection and achieves wide dynamic range imaging, supporting enhanced quantification. Typical dynamic range for the sCMOS detector is nearer 15 bits (30,000:1), based on the ratio of imaging detector full-well capacity to read noise. Figure 9 shows images of the same specimen acquired with Dragonfly and a high-performance point scanning system to illustrate the effect. True dynamic range in these point scanner images is typically limited to 8 or perhaps 10 bits (256:1 and 1024:1). The Dragonfly equivalent is around 5,000:1 in this example. If the sCMOS sensor was driven closer to saturation this could be extended to 20,000:1 or more.

9 A

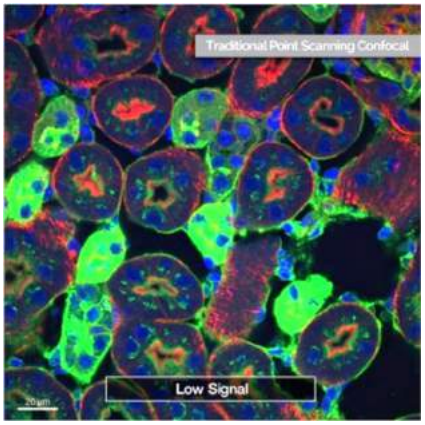

9 B

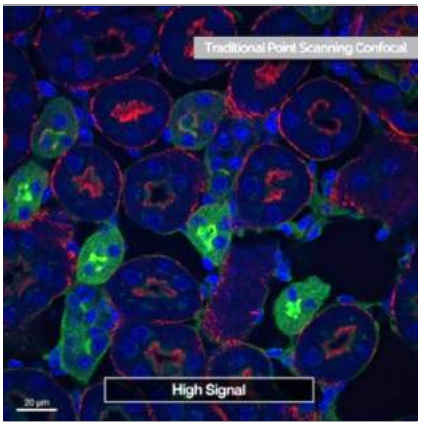

9 C

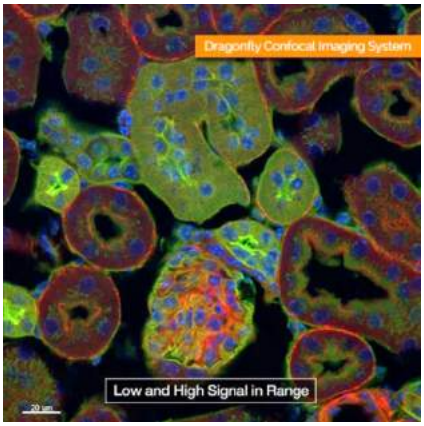

Figure 9. Point scanning confocal microscopes require two scans 9 A, 9 B to capture the full intensity range of a specimen: Low and High signals respectively. Note that high signals are saturated in the low signal image, while low intensity signals are not discernable in the high signal image.

In contrast, Dragonfly 9 C. acquires the full dynamic range of signals in a single acquisition. Dragonfly therefore speeds and simplifies visualization and quantitative analysis of such microscopic data e.g. gene expression levels.

REASON SEVEN: Photobleaching & Phototoxicity – Dragonfly is kinder to cells and has lower bleaching rates

Photobleaching of fluorophores is an inevitable consequence of fluorescence imaging. But it is a significant problem for point scanners because of the high intensities found in the focal volume. There is conjecture, and some evidence (Diaspro et al 2006), that multi-photon absorption events at point scanning power densities can accelerate bleaching; though earlier work (van der Engh and Farmer 1992) suggests that bleaching probability depends solely on the ratio of number of emitted photons to the average emission lifetime (in photons) of a fluorescent molecule. In either scenario photobleaching is considered as total loss of fluorescence of the molecule by oxidation (loss of an electron) either by reaction with the local environment or via triplet state reactions.

Some triplet state transitions do not result in loss of fluorescence, but their much longer lifetimes (0.1 to 1 µs) result in increased saturation effects. Oxidation and triplet state transitions can lead to the creation of free radicals e.g. reactive oxygen species (ROS) which are necessary in living specimens at relatively low levels. However, rapid localized ROS creation can be toxic and leads to abnormal cellular response and even to cell death. Once again Dragonfly's micro-beam illumination approach, reduces photobleaching rate, saturation effects and slows the rate of ROS release in the probe volume.

As an example of imaging live specimens, where high speed and low phototoxicity are needed, Figure 10 shows an experiment where a genetically encoded calcium indicator is used to monitor spontaneous signaling in iPSC derived cardiomyocytes.
This experiment proceeded for 15 minutes continuous imaging without obvious impact on cell health.
The large field of view of Dragonfly was especially appreciated by the user who was interested in gathering statistical data on phenotypic behaviors of these cell lines.

Lower bleaching rate has a further benefit, especially when imaging thick or delicate specimens e.g. synaptic puncta in brain tissue. The high bleaching rate and lower sensitivity of a point scanner combine to destroy fluorescence in deeper layers of the specimen before they are addressed for imaging. Dragonfly's gentler illumination and greater sensitivity combine to improve imaging quality and feasibility in such specimens.

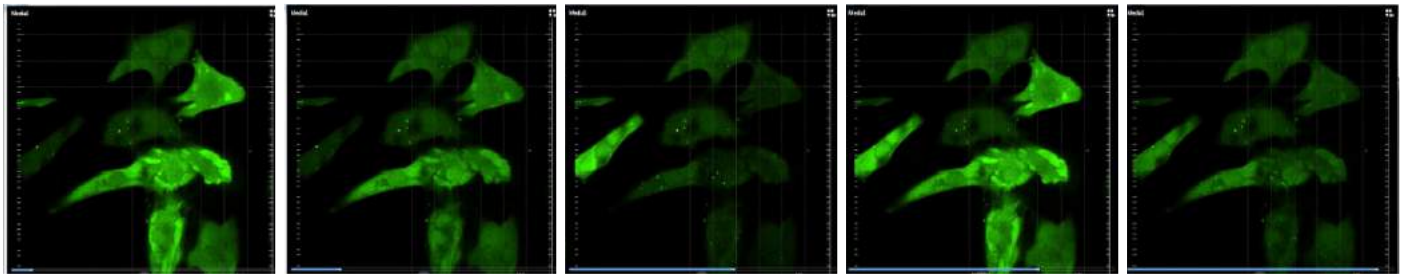

Figure 10. Images from a time series of iPS derived cardiomyocytes with a genetically encoded calcium indicator, GCaMP. Imaged on Dragonfly at 60X/1.2 magnification with 40um pinholes using iXon Ultra 888 (1024x1024) captured at 25fps. Courtesy: Dr Travis Hinston, The Pat and Jim Calhoun Cardiology Center, University of Connecticut Health Center & The Jackson Laboratory for Genomic Medicine.

REASON EIGHT: Spectral Range

Dragonfly allows operation into NIR 400–800 nm

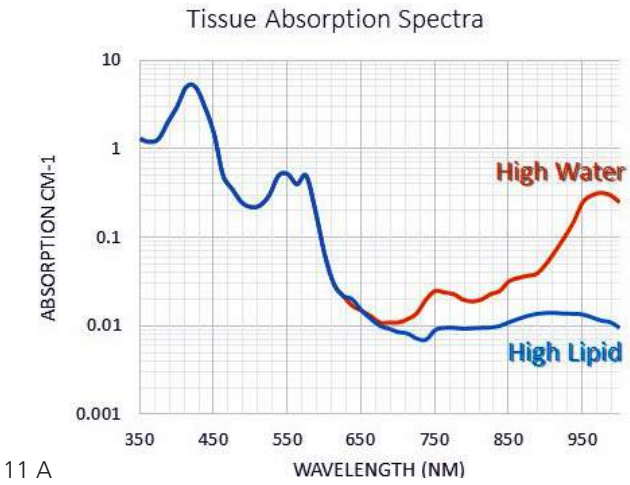

11 A

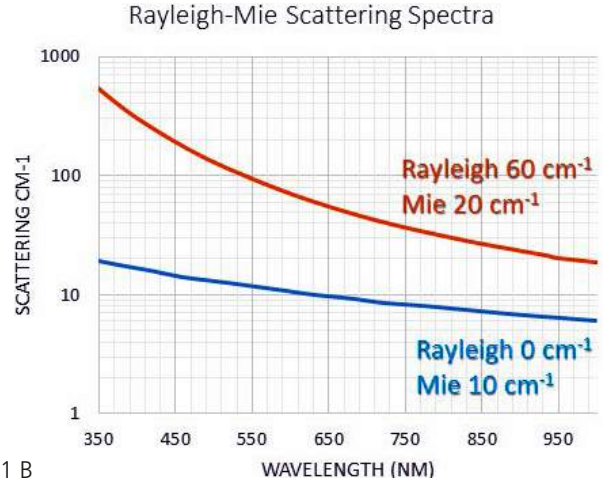

11 B

Figure 11 A. Absorption spectral curve for tissue with variable proportions of water (orange) and lipid (blue)- in the range below 650 nm, the curves are coincident.

11 B. Scattering (Rayleigh and Mie) versus wavelength in a similar range of tissues. Two extrema are shown in the lower case (blue) the curve corresponds to Rayleigh = 0.0 cm^{-1}, Mie = 10 cm^{-1}, while the upper curve (red) corresponds to Rayleigh = 60 cm^{-1}, Mie = 20 cm^{-1}. Most tissues fall within these bounds (Jacques 2013).

Most confocal microscopes (including MSD) are limited to imaging the wavelength range 425–700 nm with excitation restricted to visible lasers ranging from 400–650 nm. This is due primarily to detector photocathode limitations, but also that lasers are coupled into the illumination system via single mode optical fibers. While a single mode fiber provides an effective point source for diffraction limited point scanning, it will not efficiently couple or transmit longer wavelengths. In contrast, Dragonfly uses a multimode optical fiber in its patented illumination system, Borealis™, where light from the solid-state laser engine is coupled into a 50 µm fiber, which can support wavelengths from 350–2000 nm. The remainder of Dragonfly optics are designed to support excitation and detection in the ranges 400–800 and 425–850 nm respectively.

The importance of this extended spectral range can be appreciated by studying the wavelength dependent absorption and scattering behavior of biological tissue. Figure 11 A. shows a profile (Jacques 2013) in which the absorption coefficient, µa (cm^{-1}) is shown as a function of wavelength: orange shows the outer envelope for water absorption, while blue that for high lipid (fat) content. Figure 11 B. shows representative curves of optical scattering in tissue: the generally accepted terminology is that Rayleigh scattering refers to scattering by particles or mass density fluctuations much smaller than the wavelength of light, while Mie scattering refers to scattering by particles close or larger than the wavelength of light. Contributors to scattering are numerous and while it is possible to define generic equations combining Rayleigh and Mie, detailed spatial and biochemical structure make modelling very difficult. Direct measurements are also challenging, so that the range of estimates can be wide and different tissues show large variations with a combined range of 10–100 cm^{-1}. For simplicity in this paper, we show the envelope curves in Figure 11 B. to illustrate the intensity of the effects.

Note that the absorption and scattering profiles in Figure 11 are drawn on logarithmic scales: wavelengths 400–600 nm show absorption and scattering coefficients of more than an order of magnitude greater than the range 650–900 nm, so that working in the first NIR window is highly advantageous for imaging in-vivo and in tissue and organoid preparations but also in living preparations.

Dragonfly's wider spectral range supports NIR imaging for deeper penetration of native tissue as shown in Figure 12 and can be used to avoid auto-fluorescence which kills contrast in the visible range. The large spectral range also allows greater multiplexing of fluorophores in a single imaging acquisition protocol, which has increasing interest for e.g. transcriptome analysis. Sequential labelling cycles (Cai et al 2016) could be reduced with the larger number of imaging channels available.

Figure 12. Maximum intensity z-projection 12 A. and 3D volume rendering 12 B. of an aged rat brain slice containing oligodendrocytes and blood vessels fluorescently labeled with Invitrogen Alexa Fluor 488 dye and LI-COR® IRDye 800. Tissues like these accumulate auto-fluorescent lipofuscin pigments that create a high image background when excited and imaged with visible wavelengths.

The same z-projection 12 C. and volume rendering 12 D. of the brain slice when excited and imaged with infrared wavelengths show a greatly reduced autofluorescence background signal and a deeper imaging depth. Specimen kindly prepared by Dr. Claude Messier, University of Ottawa.

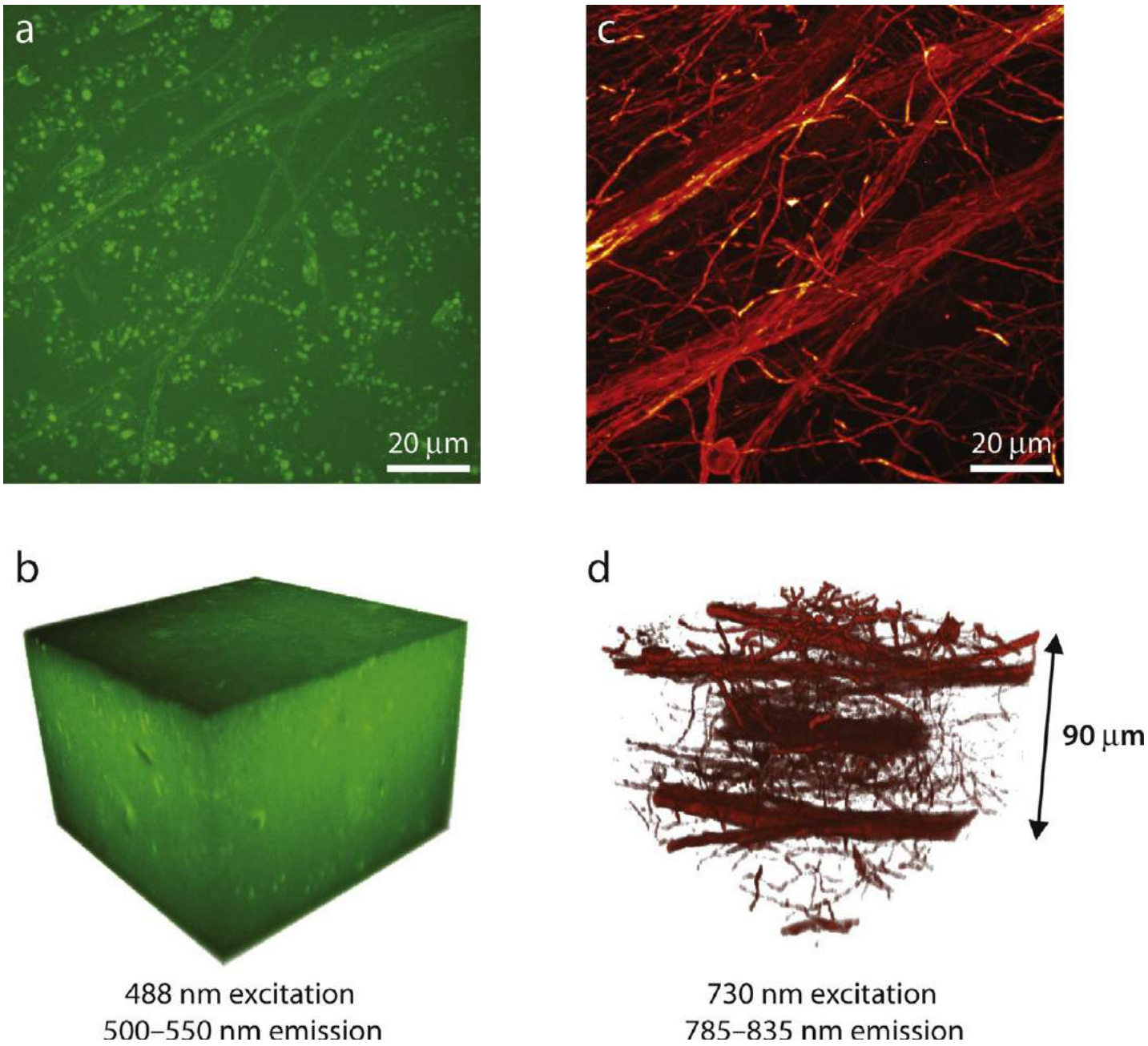

REASONS NINE and TEN:
Uniformity and Stability

Borealis™ patented illumination technology

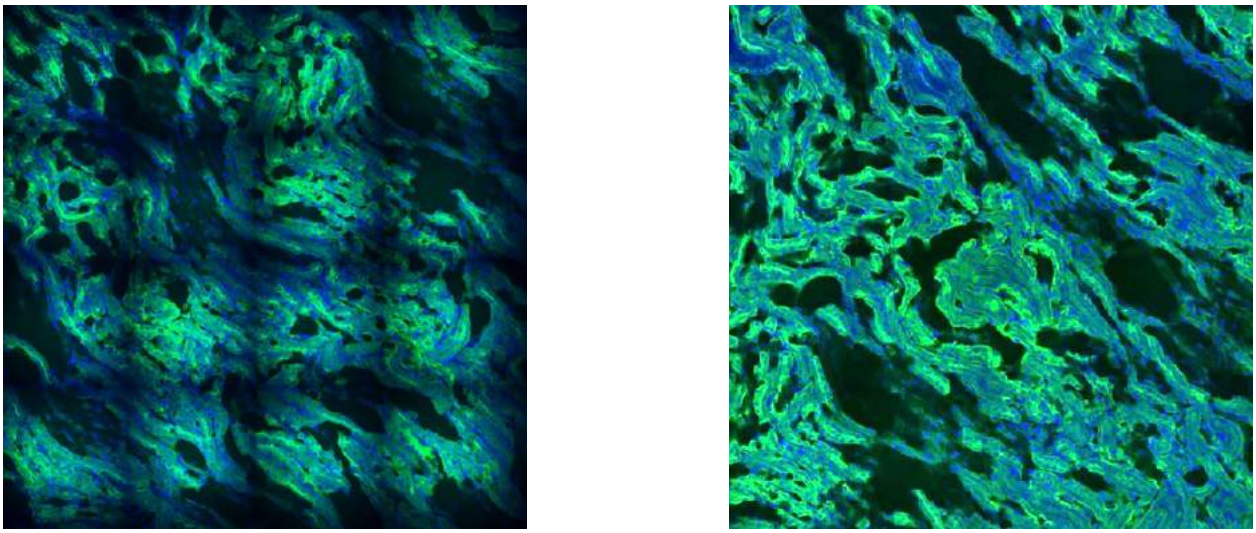

Figure 13. Uniformity and throughput: competitor MSD versus Dragonfly. Images show 4x4 tiled montage (maximum intensity projection) images from a kidney section labelled with FITC and DAPI: on the top a competitor microlens spinning disk illuminated via a single mode optical fiber shows the typical roll-off (30–40%) in the illumination field, clearly showing frame boundaries. On the bottom, we see the same specimen (different fields to avoid photobleaching artefacts) imaged with Dragonfly Borealis™ illumination, typical roll-off (~10%). The increase in brightness and uniformity is apparent.

Two further significant benefits accrue from the design of the Borealis™ illumination system: first, coupling the laser into the large multimode fiber (~200 times the area of a single mode fiber) provides higher damage threshold and improved long term stability. Unlike single mode fibers, normal levels of thermal and mechanical stress and strain have little impact on coupling efficiency with a large fiber. Second, a combination of high frequency laser homogenization and optical fiber selection to match the etendue or “optical extent” (Fischer and Tadic-Galeb 2000) of the microlens disk, deliver high throughput, low background and high spatial uniformity.

The application benefits of these features can be identified readily. Stability is important for longitudinal and comparative measurements as well as reduced instrument maintenance. Field experience with Borealis over more than five years, reveals virtually no maintenance involving re-alignment of lasers. Low background, as noted elsewhere, supports high sensitivity imaging, while illumination uniformity improves comparative quantification within the imaging field and benefits image stitching applications, which are increasingly important as we deal with larger specimens and tissues.

Point scanning confocal microscopes are not only limited in their spectral range by single mode fibers, but they can also suffer from excitation power drift. Consequently, careful monitoring and service of the laser power output will be required. This is also true for microlens spinning disk systems from other manufacturers, which use single mode fiber delivery systems. In the latter case, both uniformity and efficiency of illumination will be compromised because the manufacturer must trade throughput for uniformity, while managing the Gaussian irradiance profile typical of a single mode fiber laser beam delivery system.

Trade-offs applied in single mode excitation of microlens spinning disk and other camera-based confocals (e.g. Swept Field Confocal) require the expansion of the laser beam from a single mode (~3.5 um diameter) spot to illuminate an aperture of somewhere between 12 and 25 mm: a scaling of about 3500 to 7000 times. In fact, the scaling is often many times more than this, so that a flatter beam profile is achieved, and this results in heavy losses of throughput e.g. 90%. Although diffractive optics and specialized remapping lenses can be used to correct the beam profile with lower losses, they are usually optimized at a single wavelength, limiting their application in multi-wavelength fluorescence microscopy. Hence, Dragonfly exceeds competitor single mode systems’ performance by a factor of at least two or three in both throughput and uniformity.

REASON ELEVEN: Super-resolution

Direct Stochastic Optical Reconstruction Microscopy – dSTORM

Dragonfly supports (dSTORM) (Heilemann et al 2009), a localization methodology in which the blinking of organic dyes is enhanced by reductant substrates such as MEA (mercaptorethylamine). As with all localization-based super-resolution methods, dSTORM excites a sparse sub-population of single molecules in a time series and identifies their position to sub-pixel precision by fitting a (Gaussian) point spread function to each detected fluorophore. Accumulation of the localizations creates a super-resolution pointilliste image. Accuracy depends on SNR (and background) so high laser power densities (>1 kW cm^{-2}) are needed to extract a high number of photons from the molecule in each frame and return molecules to a dark state quickly. To support this kind of experiment, the Dragonfly Borealis™ illumination system is designed with four motorized illumination zooms from 1X to 6X (1X–36X power density). This allows the same laser used for confocal, widefield and TIRF to be applied to dSTORM imaging. The benefits of using flat field illumination, like Borealis™, for super-resolution have recently been emphasized by Douglass et al (2016). See Figure 14 for an example data set from a dSTORM experiment performed with Dragonfly.

Recently researchers have developed probes whose fluorescence blinking results from transient DNA-DNA interactions (Jungmann et al 2014): DNA-Paint requires lower power densities because the blinking rate is not driven by bleaching molecules into dark states, but by the relative affinity between probe and target. This technique offers significant promise and is well matched to Dragonfly capabilities.

To explore the 3rd dimension in super-resolution localization, Dragonfly provides a motorized astigmatic lens to create a calibrated asymmetric distortion of the single molecule PSF, which varies with axial defocus (Mlodzianoski et al 2009). The asymmetry encodes positive and negative axial offset differentially in X and Y dimensions and is supported in many third-party localization analysis tools e.g. Thunderstorm (Ovesny et al 2014).

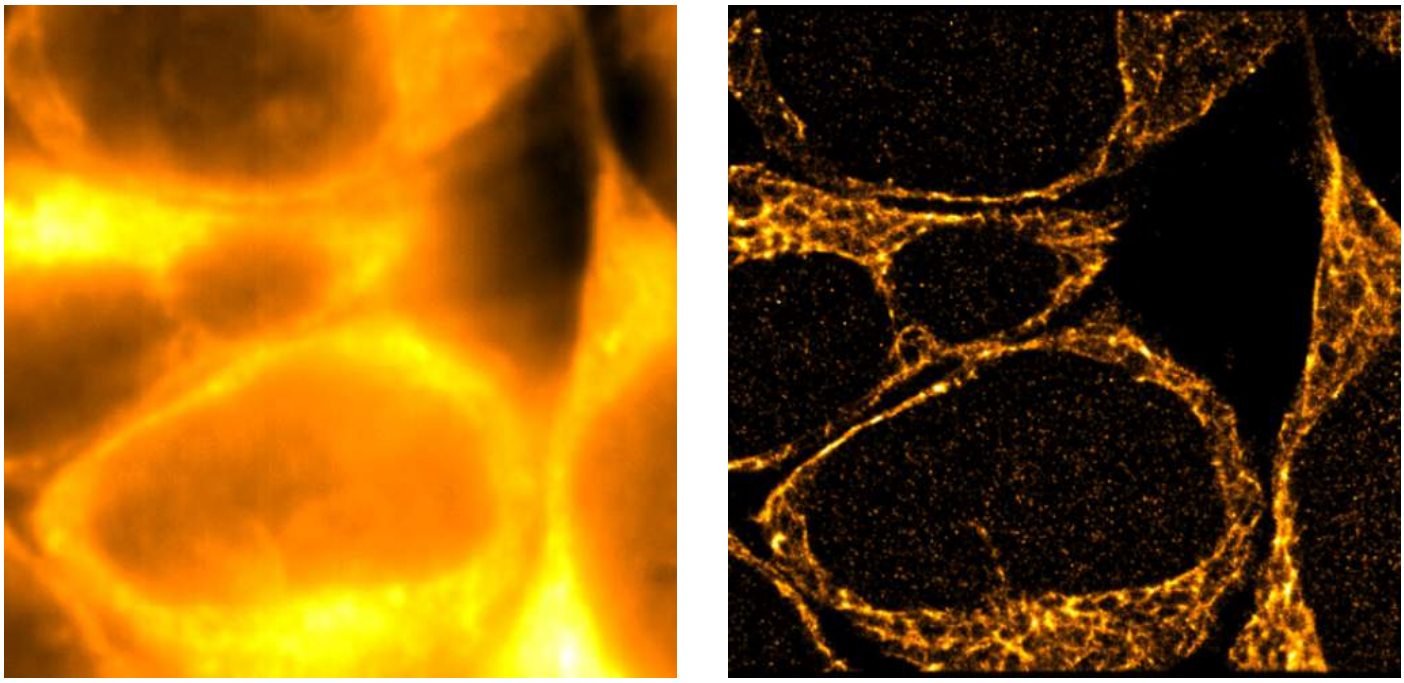

Figure 14. Microtubules in HeLa cells labelled with anti-TOMM20 Alex647, were buffered with MEA (beta mercaptorethylamine) and imaged on Dragonfly in widefield mode with a 638 nm 140 mW laser, set for maximum excitation power density (~2 kW cm-2). 15,000 frames were acquired on the iXon Ultra 888 center cropped to 256x256 pixels with imaging zoom at 2X and 50 frames per second in overlap mode, giving an effective exposure of ~20 ms per frame. The resulting data was processed with Thunderstorm. Left is the accumulated widefield image series. Right is the fitted pointilliste image exhibiting enhancement to an estimated 40 nm resolution, FWHM. Drift correction was not applied. Specimen courtesy of Dr Nicolas Touret, University of Alberta.

REASON TWELVE: Super Resolution Radial Fluctuations – SRRF-Stream:

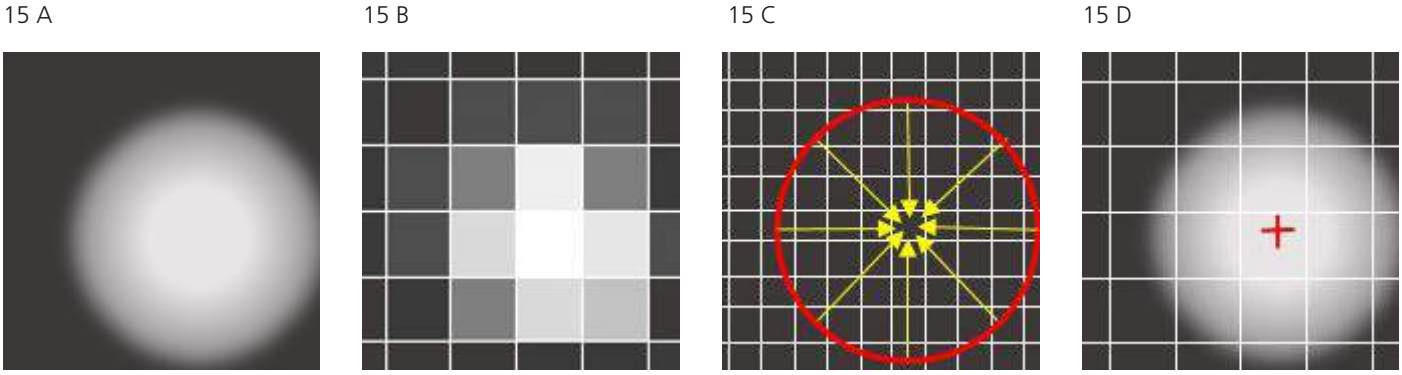

Figure 15. The concept of radial symmetry for localization of fluorescent emitters (after Parthasarathy). In SRRF, the degree of radial symmetry in local intensity fluctuations is referred to as "radiality" and radiality is interpreted as the probability of the presence of an emitter. Hence the temporal correlation of radiality on a super-sampled grid provides a weighted super-resolution estimate of the emitter distribution.

Stochastic fluctuation analysis (SFA), such as SOFI (Dertinger 2009) and SRRF (Gustafsson et al 2016), depends on the analysis of image time series. Usually short exposures are used to enable relatively fast sampling. The value assigned to an output pixel depends on both the original brightness and the correlation coefficient resulting from analysis of temporal intensity fluctuations in the pixel. Background tends to be poorly correlated and so significant gains in contrast can be won. In SOFI, improved resolution is derived from higher order cumulants: these are statistical moments of the time series data. In SRRF, resolution gains are achieved from continuous interpolation of the radiality field. Radiality is computed from the local radial gradient (Parthasarathy 2012) and B-spline interpolation onto a super-sampled pixel grid. High levels of radial symmetry are indicative of the locale of fluorescence emitters (see Figure 15). SFA methods handle high fluorophore densities, and function with conventional fluorescent molecules, making them applicable to widefield, confocal and TIRF image data. In terms of resolution and light dose SFA is competitive with structured illumination microscopy (SIM) (Gustafsson M 2000).

In SRRF, the number of images per sequence can be varied to trade spatial and temporal resolution. This is especially useful for live cell studies where phototoxicity is a concern. Typically, 10 times the light dose is required to double resolution. The SRRF algorithm conveniently deals with dSTORM data as well as short time burst and so it provides a flexible and powerful adjunct to the super-resolution toolbox.
To exploit SRRF optimally, we have created SRRF-Stream, a GPU-accelerated implementation which streams images from the camera direct to GPU for near real-time processing. SRRF-Stream is implemented with iXon Ultra cameras (Browne et al 2017). Integration into Dragonfly/Fusion will be released in the fall of 2017. To appreciate the speed of SRRF-Stream refer to Table 3, where processing times are shown to be in line with acquisition times and hence "real time" super-resolution performance.

NVidia GPU	Data size uint16	SRRF-Stream ms
K5000	512x512x100	478
	1024x1024x100	1878
	2048x2048x100	7527
M4000	512x512x100	284
	1024x1024x100	1115
	2048x2048x100	4422

Table 3. SRRF-Stream performance for pixel zoom 4X, i.e. output contains 16 times more pixels. Andor's SRRF-Stream has been optimized not only for execution, but also for data flow to and from the GPU, enabling integration with camera acquisition.

Early experience with SRRF-enabled cameras and Dragonfly is encouraging and we present two examples here. In Figure 16 A we explore resolution vs number of frames processed in a live cell TIRF time series. Comparing conventional TIRF with SRRF-TIRF images of microtubule dynamics show a significant reduction in background, while mean lateral resolution, measured by FRC (Fourier ring correlation) improves asymptotically to around 75 nm or better after 1000 frames.

Looking at FRC convergence in sub-areas of the image and referring to the blue line in Figure 16 A, we see that some sub-areas of the image achieve sub-100 nm resolution after less than 100 frames. Suggesting that dynamic live cell imaging can achieve this resolution at around 1 composite frame per second under the right conditions.

16 A

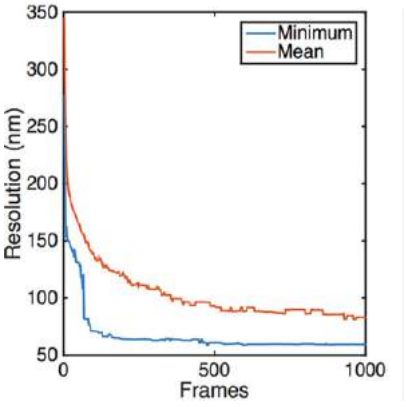

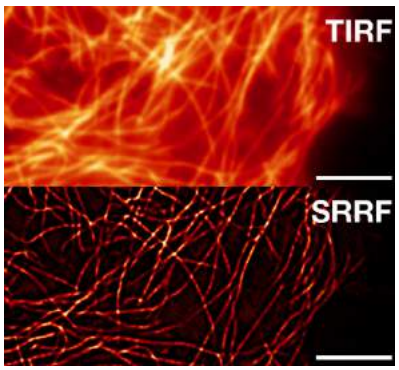

16 B

Figure 16 A. The evolution of FRC (Fourier Ring Correlation) resolution with number of frames in the SRRF-Stream time series. Data was acquired with an iXon EMCCD at 10 ms exposure, running qt ~100 fps using a Nikon 60X/1.49 TIRF objective, microtubules visualized with GFP excited at 488 nm. The image was divided into 32x32 pixel sub-arrays and FRC computed on each: Mean (red) shows the average from all ROI's analyzed, while Minimum (blue) shows the best resolution of the ROI group.

16 B. SRRF functions across modalities and fluorophores. Averaged widefield image of fixed cell specimen with anti-tubulin label shown in blue. Below is the SRRF-Stream result from processing the same 100 frames Data acquired on Dragonfly with iXon Ultra 888, Nikon 60X/1.49 TIRF lens 2X magnification.

In the next experiment our goal was test the behavior of the SRRF algorithm with fixed tissue and conventional fluorophores in confocal imaging. For Figure 17, we gathered 100 frames at 512x512 from iXon Ultra 888 with high SNR at exposure time 30 ms and pixel size ~196 nm in three fluorescent channels from a fixed kidney section. The SRRF-Stream algorithm was applied to the data series with a pixel magnification of 8 times, resulting in an image of 4096x4096 with pixels ~25 nm.

As can be observed the striation in vessel walls (red channel) which might be considered as ambiguously separated features in the confocal images are clearly separated in the SRRF images. Using the full-width half height ruler, commonly applied in the literature, the feature width is measured at ~ 100 nm.

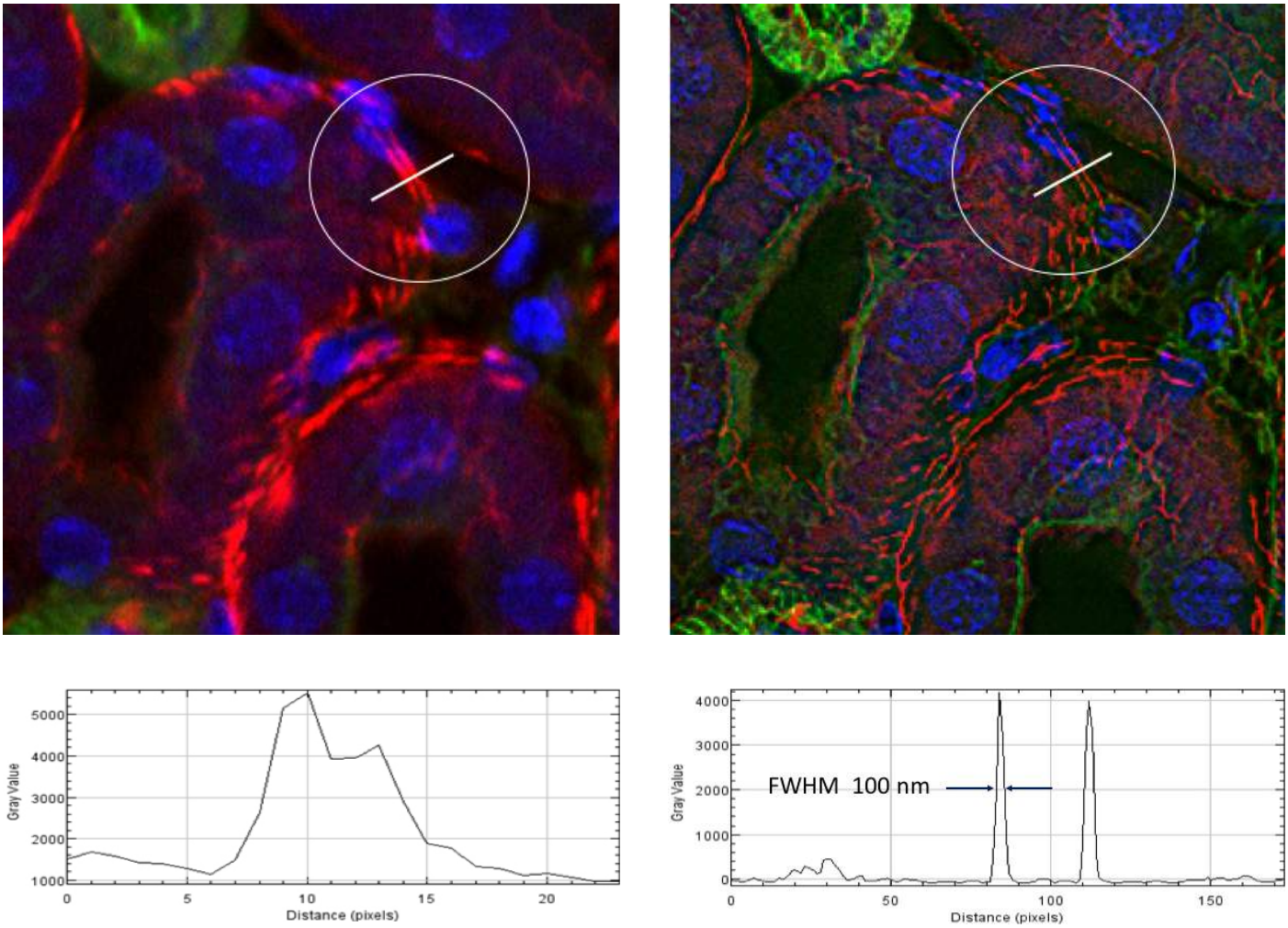

Figure 17. Confocal data from a triple labelled kidney section acquired with Dragonfly 40 µm pinhole, Planapo 60X/1.4 oil objective, iXon 888 at 1.1X magnification. Bottom: 256x240 cropped from 512x512 raw confocal data is contrasted with 1024x960 cropped from 2048x2048 SRRF-Stream image processed from 100 frames. Top: line profiles of highlighted features (like scaling), showing 100 nm FWHM from striated features in kidney vasculature from 4096x4096 SRRF-Stream result.

Discussion

Dragonfly is a powerful, flexible tool which can be adapted to your questions

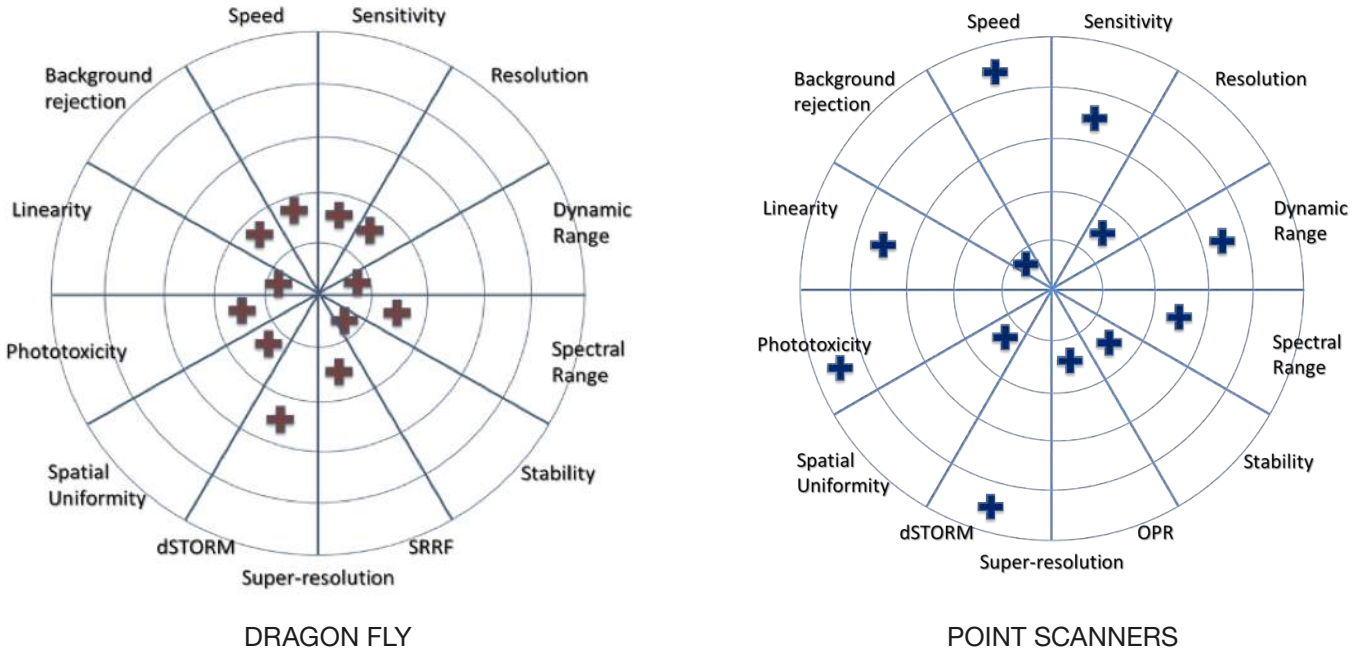

Figure 18. The Confocal Bullseye – the perfect confocal microscope would score Twelve bullseyes – one per feature. Comparing Dragonfly to a point scanner on a scale one to five in each category, puts Dragonfly in front by some margin. Would you score the same way? We would be interested to hear your opinions? Note that in the Point Scanners bullseye, OPR refers to optical photon reassignment, such as that used in Zeiss AiryScan™. Other competitive methods include Leica's Hyvolution which uses a sub-Airy pinhole with deconvolution.

Life science research has entered a new era: as understanding deepens, questions become more complex and require imaging tools which can bridge scales from nm to mm. Speed, throughput, resolution and high volumes of quantifiable data are essential components in this endeavor. Dragonfly is designed as a high-resolution imaging platform which delivers performance and value to both multi-user and single investigator labs. Dragonfly achieves performance across multiple imaging modes without compromise because the fundamental requirements are common: mechanical and optical stability; efficient and well-controlled illumination; optimized detection pathways; careful management of stray light; sensitive detectors; and high performance, easy to use software. Understanding these principles allowed us to develop a product which exceeds or challenges competitive products in every feature of performance.

In this white paper, we have compared Dragonfly with point scanning and focused on technologies rather than individual instruments. We have discussed strengths and weakness of both technologies and contrasted Dragonfly with previous generation MSD. Some may argue that we should consider light sheet as a new and competing technology, but such a comparison is difficult because light sheet is still an emergent technology and not widely available as a standard tool, but no doubt this technology will mature. Dragonfly does not offer spectral imaging, at least for now, and if this is an important tool for your research, we ask you to consider the wider spectral range as a means of increasing multiplex, if that is the goal. Of course, there is no perfect confocal microscope, but we summarize the performance factors we have considered here, with Figure 18 in which the bullseye represents perfection. With this, we suggest that Dragonfly marks a significant step towards the goal of improving performance, throughput and data quality. These are key factors in evaluating instrumentation for the future of research in the life sciences.

Dragonfly is an extremely capable confocal, widefield and TIRF imaging platform and it can be equipped for two modes of super-resolution imaging. GPU-accelerated image processing and real-time 4D visualization are key tools for modern research, enabling rapid exploration and interpretation. This flexibility delivers the functionality you need to ask biological questions in the right context, and that may mean expressing the biology of interest in more than one model organism or specimen preparation. Dragonfly is uniquely adaptable to these studies and specimen types. While we have focused on confocal performance versus point scanning systems here, the broader capabilities are summarized in Table 4, where we show which Dragonfly features benefit the kinds of specimen types in wide spread use today.

Let **Dragonfly** be the next confocal system in your lab or core facility, and contact Andor for more information or to arrange a demonstration!

Table 4. shows how Dragonfly features map onto specific kinds of specimen and imaging experiment.

Specimen type	SM Tracking	Extra-cellular	SMLM	Yeast	Live cell	Expansion	Embryo			Tissue	Cleared tissue
Feature			dSTORM DNA-PAINT				Zebra fish	Worms	Drosophila		
Confocal 40			✔	✔	✔	✔	✔	✔	✔	✔	✔
Confocal 25				✔	✔	✔	✔	✔	✔	✔	✔
Widefield	✔	✔	✔	✔	✔						
Widefield + Astigmatic	✔		✔								
TIRF	✔	✔	✔	✔	✔						
Deconvolution	✔	✔		✔	✔	✔	✔	✔	✔	✔	✔
Camera Zoom	✔	✔	✔	✔	✔	✔	✔	✔	✔	✔	✔
Dual Camera	✔	✔	✔	✔	✔	✔	✔	✔	✔	✔	✔
Illumination Zoom	✔	✔	✔								
SRRF-Stream	✔		✔	✔	✔	✔	✔	✔	✔	✔	✔

References

01. Pawley J., "The 39 Steps: A Cautionary Tale of Quantitative 3-D Fluorescence Microscopy" Biotechniques 28(5):884–6, 888, June 2000

02. Tsien R.Y., Ernst L., Waggoner A. "Fluorophores for Confocal Microscopy: Photophysics and Photochemistry" Chapter 16, Handbook of Biological Confocal Microscopy, Third Edition, edited by James B. Pawley, Springer Science+Business Media, LLC, New York, 2006

03. Oreopoulos J., Berman R., Browne M., "Spinning-disk confocal microscopy: present technology and future trends" Chapter 9, Quantitative Imaging in Cell Biology, Vol 123, edited by Waters J., Wittman T., ISBN: 9780124201385, Academic Press 2014

04. Dickinson, M., Bearman, G., Tille, S., Landsford and Fraser, S. "Multi-spectral imaging and Linear Unmixing add a whole new dimension to Laser scanning fluorescence microscopy", Biotechniques 31(6): 1272–1278, 2001

05. "Photomultiplier Tubes: Basics and Applications" Third Edition (3a), Editorial Chief, Toshikazu Hakamata, Hamamatsu Photonics KK, 2007

06. Becker W., "Advanced Time-Correlated Single Photon Counting Techniques", ISBN-10 3–540–26047–1, Springer Verlag, Berlin Heidelberg, 2005

07. Coates C., Fowler B. and Holst G., "Scientific cmos technology: A high-performance imaging breakthrough," http://www.scmos.com/files/low/scmos white paper 2mb.pdf (2009)

08. Basden A.G., "Analysis of EMCCD and sCMOS readout noise models for Shack-Hartmann wavefront sensor accuracy" arXiv:1506.07929 [astro-ph.IM]

09. Egner A., Andresen V., Hell S., "Comparison of the axial resolution of practical Nipkow-disk confocal fluorescence microscopy with that of multifocal multiphoton microscopy: Theory and experiment" J. Microsc, 206, 24–32, 2002

10. Shimozawa T., Yamagata K., Kondo T., Hayashi S., Shitamukai A., Konno D., Matsuzaki F., Takayama J., Onami S., Nakayama H., Kosugi Y., Watanabe T., Fujita K., Mimori-Kiyosue Y., "Improving spinning disk confocal microscopy by preventing pinhole cross-talk for intravital imaging", PNAS, 110, 9, 3399-3404, 2013

11. Wang E., Babbey C.M., Dunn K.W. "Performance comparison between the high-speed Yokogawa spinning disc confocal system and single-point scanning confocal systems" J. of Microscopy, The Royal Microscopical Society, 218, 148–159, 2005

12. Diaspro A., Chirico G., Usai C., Ramoino P., Dobrucki J. "Photobleaching" Chapter 39, Handbook of Biological Confocal Microscopy, Third Edition, edited by James B. Pawley, Springer Science+Business Media, LLC, New York, 2006

13. van der Engh G., Farmer C., "Photo-Bleaching and Photon Saturation in Flow Cytometry" Cytometry 13:669–677, 1992

14. Jacques S.L., "Optical properties of biological tissues: a review" Phys. Med. Biol. 58, R37–R61, 2013

15. Sha S., Lubeck E., Zhou W., Cai L., "In Situ Transcription Profiling of Single Cells Reveals Spatial Organization of Cells in the Mouse Hippocampus" Neuron 92, 342–357, October 19, 2016, Elsevier Inc

16. Fischer R.E., Tadic-Galeb B., "Optical System Design", SPIE Press, ISBN 0–07–134916–2, McGraw-Hill, 2000

17. Heintzmann R., Sheppard C.J.R., "The sampling limit in fluorescence microscopy", Micron 38, 145–149, 2007

18. Wilson T., "Resolution and Optical Sectioning in the Confocal Microscope", J. Microsc., 244, 113–121, Royal Microscopical Society, 2011

19. Sheppard C.J.R., Gan X., Gu M., Roy M., "Signal-to-Noise Ratio in Confocal Microscopes" Chapter 22, Handbook of Biological Confocal Microscopy, Third Edition, edited by James B. Pawley, Springer Science+Business Media, LLC, New York, 2006

20. Dertinger T., Colyera R., Iyera G., Weiss S., Enderlein J., "Fast, background-free, 3D super-resolution optical fluctuation imaging (SOFI)" PNAS, vol. 106, no. 52, pp 22287–22292, 2009

21. Heilemann M., van de Linde S., Mukherjee A., Sauer M., "Super-Resolution Imaging with Small Organic Fluorophores" Angew. Chem. Int. Ed. 48, 6903–6908, 2009

22. Gustafsson N., Culley S., Ashdown G., Owen D., Pereira P., Henriques R., "Fast live-cell conventional fluorophore nanoscopy with ImageJ through super-resolution radial fluctuations", Nature Communications 7, Article number: 12471, 2016

23. Parthasarathy R., "Rapid, accurate particle tracking by calculation of radial symmetry centers", Nature Methods 9, 7 pp 724–726, 2012

24. Douglass K., Sieben C., Archetti A., Lambert A., Manley S., "Super-resolution imaging of multiple cells by optimized flat-field epi-illumination", Nature Photonics 10, 705–708, 2016

25. Ovesny M., Krizek P., Borkovec J., Svindrych Z., Hagen G., "ThunderSTORM: a comprehensive ImageJ plug-in for PALM and STORM data analysis and super-resolution imaging", Bioinformatics, Oxford Uni Press, Vol. 30, 16, pp 2389–2390 2014

26. Jungmann R., Avendaño M., Woehrstein J., Dai M., Shih W., Yin P., "Multiplexed 3D cellular super-resolution imaging with DNA-PAINT and Exchange-PAINT", Nat. Methods, 11, 3, 313–318, 2014

27. Mlodzianoski, M., Juette M., Beane G., Bewersdorf J., "Experimental characterization of 3D localization techniques for particle-tracking and superresolution microscopy" Optics Express Vol 17, 10, pp 8264–8277, 2009

28. Gustafsson M, "Surpassing the lateral resolution limit by a factor of two using structured illumination microscopy", J. Microsc., 198, 82–87, 2000

29. Browne M., Gribben H., Catney M., Coates C., Wilde G., Culley S., Henriques R., "Multimodal Super-resolution Microscopy through SRRF". Proceedings Focus on Microscopy, Bordeaux, April 9–12, 2017

30. Puthenveedu M., Lauffer B., Temkin P., Vistein R., Carlton P., Thorn K., Taunton J.,. Weiner O., Parton R., von Zastrow M., "Sequence-Dependent Sorting of Recycling Proteins by Actin-Stabilized Endosomal Microdomains", Cell 143, 761–773, November 24, 2010

Head Office
7 Millennium Way
Springvale Business Park
Belfast BT12 7AL
Northern Ireland
Tel: +44 (0)28 9023 7126
Fax: +44 (0)28 9031 0792

North America
300 Baker Avenue
Suite 150
Concord, MA 01742
USA
Tel: +1 860-290-9211
Fax: +1 860-290-9566

Japan
5F IS Building
3-32-42 Higashi-Shinagawa
Tokyo 140-0002
Japan
Tel: +81-(0)3-6732-8968
Fax: +81-(0)3-6732-8939

China
Unit 1, Building A,
No. 66 Zhufang Road,
Haidian District,
Beijing 100085
P. R. China
Tel: +86 (0)10-8271-9066
Fax: +86 (0)10-8271-9055

Find us on

ANDOR
an Oxford Instruments company

OXFORD INSTRUMENTS
The Business of Science®